Improvement of Hydrodynamics Performance of Naphtha Catalytic Reforming Reactors Using CFD

Mohammadikhah, Rasool*[+]; Zahedi Abghari, Sorood; Ganji, Hamid; Ahmadi Marvast, Mahdi

Process Development & Control Group, Process Development & Equipment Technology Division, Research Institute of Petroleum Industry (RIPI), Tehran, I.R. IRAN

ABSTRACT: *Due to high applicability of the fixed bed catalytic naphtha reforming reactors, hydrodynamic features of this kind of reactors with radial flow pattern are improved in this work by utilising computational fluid dynamics technique. Effects of catalytic bed porosity, inlet flow rate and flow regime through the bed on the flow distribution within the system are investigated. It is found that the first reactor among three fixed bed reactors in series is working inappropriately. It is due to the effects of recirculating flow on the hydrodynamics. In addition, flow distribution at the end of each bed is discovered to be non-uniform. By applying computational fluid dynamics technique to the system and manipulating effective parameters, not only vortices are removed at the end of each bed, but also flow distribution through the first reactor is considerably improved. A new internal modification for all reactors is proposed, which allows reactors to become overloaded with the catalyst. Subsequently, inlet flow rate can rise by 10-15 per cent over its current value.*

KEY WORDS: *CFD, Capacity enhancement, Flow distribution, Improvement, Pressure drop, Turbulence, Fixed bed, Catalytic reforming reactor, Uniformity.*

INTRODUCTION

Recently, researchers have paid attention to making CFD tools ready for modelling industrial processes involving reactors, vessels, and so on [1]. The role of naphtha catalytic reforming, which contributes approximately 50-80 volume per cent to the petrol pool in the refinery, is as crucial now as it has been for over the 70 years of its commercial use [2, 3]. It converts low-octane straight run naphtha to petrol with octane number higher than 90 degrees [4]. Many of gas phase reactions like naphtha catalytic reforming are carried out through radial fixed bed reactor rather than axial/vertical fixed bed reactor due to lower pressure drop [1]. In radial fixed bed reactor, feed stream flows both axially and radially, subsequently creating some flow distribution problems [5,6]. In an ordinary way, catalyst is charged to free space (annulus compartment) between the scallops (inner screen) and the perforated centre pipe (outer screen), as can be seen in Fig. 1. Each scallop is a perforated half cylinder with a small diameter.

Catalytic synthesis of ammonia was the first case in which radial flow fixed bed reactor was used, and it has ever since been used for catalytic reforming, desulphurisation and nitric oxide conversion [7-9]. Earlier works showed that under a perfect radial flow distribution, direction

* *To whom correspondence should be addressed.*
+ *E-mail: mohammadikhah@ripi.ir*
1021-9986/14/3/ 8/$/2.80

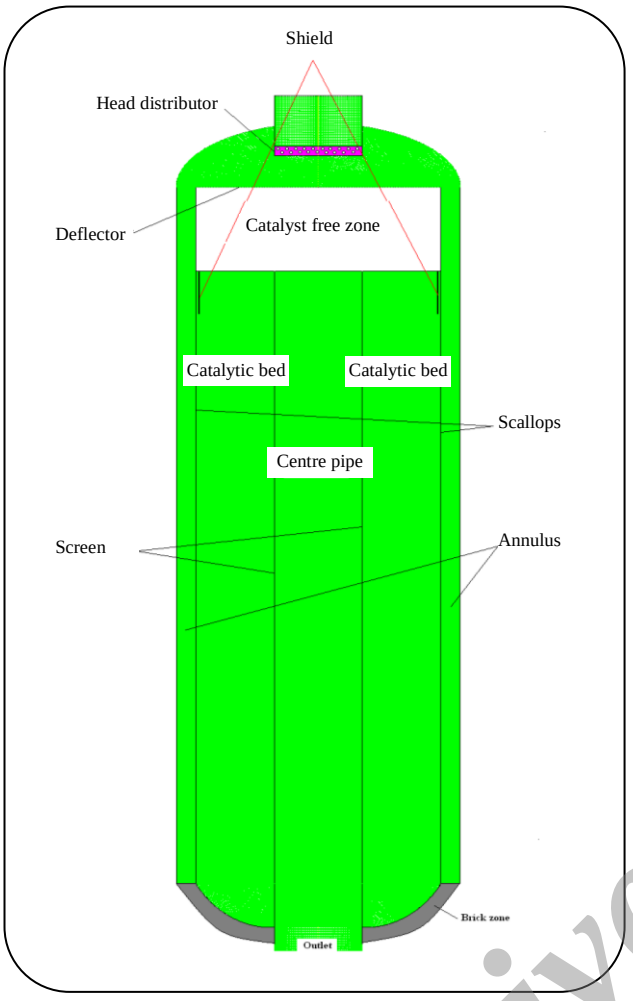

Fig. 1: The first CRU reactor with internal specifications.

of the radial flow (i.e. centripetal or centrifugal/ upward or downward) has a significant effect on the conversion [10-12]. Effects of mal-distribution and flow direction on the reactor performance were investigated [13]. *Chang & Calo* [14] concluded that the optimal flow distribution in a radial fixed bed reactor could be achieved by adjusting the reactor dimensions. In a particular study on the radial flow fixed bed reactor, a significant portion of catalytic bed was not effectively utilised [15]. Such a scenario can be eliminated by using tight packing of the catalyst particles, i.e. dense loading [16]. A highly important parameter, which affects the flow uniformity, is the ratio of the cross-sectional area of the centre pipe to that of annular channel [17,18]. *Bolton et al.* [19] performed experimental determination and CFD analysis on flow distribution in a fixed bed reactor with a novel design. None of the above studies was for a commercial/industrial plant, due to, perhaps, the limitation in the computational facility and prohibitively expensive CFD calculation. *Ranade* [20] investigated only hydrodynamics of a simplified commercial system and succeeded in making uniform flow distribution, as we did [21]. Capacity enhancement of naphtha catalytic reforming reactors and its limitations were examined [22]. An extensive CFD study on the turbulence models capable of successful pressure drop prediction through naphtha catalytic reforming reactors was investigated [23]. A reaction-free CFD model probed heat transfer in certain CRU reactors [24]. Further simulation showed that even considering reactions through catalytic beds in addition to heat transfer, the velocity profile remains unchanged [25]. The main aim of the present work is to improve reactor performance in an industrial scale with the help of a comprehensive heat and reaction-free CFD analysis.

Process flow description

Selected Catalytic Reforming Unit (CRU) consists of three radial flow fixed bed reactors in series. Operational and geometrical characteristics of all reactors are listed in Tables 1 and 2 respectively. Operational variables for both design and working (current) conditions are incorporated into Table 1.

Geometry and grid generation

Two-dimensional and three-dimensional geometries are constructed just as the real system by commercial Gambit.2.3 (FLUENT. Inc, USA). Commonly, we prefer to follow calculation in three dimensions (3D) because swirl flow can be detected only within three dimensions. After ascertaining that there is no swirl flow through the system, two-dimensional (2D) geometries can widely be used, as done in this study. The final grid is fine enough to remove mesh dependency of velocity profile and CFD results and to capture wall treatment. A commercial CFD solver, FLUENT.6.3, is used to solve Navier-Stokes equations of motion throughout fluid domain.

Governing equations

Continuity equation, valid for 2D-axially symmetric flow, is defined as follows:

$$\frac{\partial \rho}{\partial t}+\frac{\partial}{\partial x}\left(\rho v_x\right)+\frac{\partial}{\partial r}\left(\rho v_r\right)+\frac{\rho v_r}{r}=S_m \qquad (1)$$

Table 1: Operational variables of selected CRU. The shadowed rows show the design data.

Variable	1st reactor	2nd reactor	3rd reactor
Inlet Pressure (Psig)	420	402	398
	445	415	395
Outlet Pressure (Psig)	418	398	390
	428	406	378
Inlet Temperature (°F)	940	940	940
	1000	1000	1000
Outlet temperature (°F)	828	904	936
	911	981	998
Maximum endurable pressure (Psig)	1193	1118	1056

Table 2: Geometrical details of catalytic reforming reactors.

Variable	1st reactor	2nd reactor	3rd reactor
Diameter (in)	78	90	102
Height (ft)	18	19-6"	23-3"
Distributor open area (%)	~10	~10	~10
Scallops open area (%)	~78	~79	~73
Screen open area (%)	36	36	36
Centre pipe open area (%)	~1.4	~1.53	~1.4
Thickness (mm)	83	89	95.5

Where S_m is the mass added to the continuous phase via disperse phase and is zero in this particular case. Axial and radial momentum conservations are given by:

$$\frac{\partial}{\partial t}\left(\rho v_x\right)+\frac{1}{r}\frac{\partial}{\partial x}\left(r\rho v_x v_x\right)+\frac{1}{r}\frac{\partial}{\partial r}\left(r\rho v_r v_x\right)= \quad (2)$$
$$-\frac{\partial p}{\partial x}+\frac{1}{r}\frac{\partial}{\partial x}\left[r\mu\left(2\frac{\partial v_x}{\partial x}-\frac{2}{3}\left(\nabla.\vec{v}\right)\right)\right]+$$
$$\frac{1}{r}\frac{\partial}{\partial r}\left[r\mu\left(\frac{\partial v_x}{\partial r}+\frac{\partial v_r}{\partial x}\right)\right]+F_x$$

$$\frac{\partial}{\partial t}\left(\rho v_r\right)+\frac{1}{r}\frac{\partial}{\partial x}\left(r\rho v_x v_r\right)+\frac{1}{r}\frac{\partial}{\partial r}\left(r\rho v_r v_r\right)= \quad (3)$$
$$-\frac{\partial p}{\partial r}+\frac{1}{r}\frac{\partial}{\partial r}\left[r\mu\left(2\frac{\partial v_r}{\partial r}-\frac{2}{3}\left(\nabla.\vec{v}\right)\right)\right]+$$
$$\frac{1}{r}\frac{\partial}{\partial x}\left[r\mu\left(\frac{\partial v_r}{\partial x}+\frac{\partial v_x}{\partial r}\right)\right]-2\mu\frac{v_r}{r^2}+\frac{2}{3}\frac{\mu}{r}\left(\nabla.\vec{v}\right)+\rho\frac{v_z^2}{r}+F_r$$

Where

$$\nabla.\vec{v}=\frac{\partial v_x}{\partial x}+\frac{\partial v_r}{\partial r}+\frac{v_r}{r} \quad (4)$$

The term F in Eq.(2) and Eq.(3) symbolises the momentum source term induced by body forces or here by porous media resistance:

$$F_i=-\left(\sum_{j=1}^{3}D_{ij}\mu v_j+\sum_{j=1}^{3}C_{ij}\frac{1}{2}\rho|v|v_j\right) \quad (5)$$

The first term on the right hand is engaged in F as viscous loss and the second as inertial loss. D and C are prescribed matrices, able to switch to a scalar in case of isotropic porous environment. For homogeneous porous media, Eq. (5) is reduced to:

$$F_i=-\left(\frac{\mu}{\alpha}v_i+C\frac{1}{2}\rho|v|v_i\right) \quad (6)$$

There are somehow a few theoretical, empirical or semi-empirical models for evaluating pressure drop

across porous media [26-28]. The most used model is the Ergun equation that correlates the pressure drop with velocity magnitude, as demonstrated beneath:

$$\frac{\Delta P}{L}=\frac{150\mu}{D_p^2\phi_p^2}\frac{(1-\varphi)^2}{\varphi^3}v+\frac{1.75\rho}{D_p\phi_p}\frac{(1-\varphi)}{\varphi^3}v^2 \quad (7)$$

Alternatively, in a simpler form:

$$\frac{\Delta P}{L}=\frac{\mu}{\alpha}v+\frac{1}{2}C\rho v^2 \quad (8)$$

Permeability and inertial loss coefficient may theoretically be determined [29]:

$$C=\frac{3.5}{D_P}\frac{(1-\varphi)}{\varphi^3} \qquad \alpha=\frac{D_P^2}{150}\frac{\varphi^3}{(1-\varphi)^2} \quad (9)$$

RESULTS AND DISCUSSION

Effect of the coarsening/fining of the mesh (mesh size) on the results should be investigated to attain valid CFD analysis to be referable afterwards. For this purpose, five different grids were used. The grids named 1, 2, 3, 4 and 5 in Fig. 2 have a node distribution identical to 162×27, 223×40, 304×56, 1399×189 and 670×108 respectively, which are in correspondence with an $x\times y$ lattice. The thus obtained results reveal that the grids finer than 670×108 distributed points do not affect the velocity profile. The obtained profile through the bed section is almost as linear as it is through the beds packed by dense loading. Therefore, the fluid traverses the bed via diffusion mechanism with laminar regime. For this reason, turbulence generation and dissipation will be suppressed henceforth, unless for those highlighted.

Design conditions

Design operational conditions can be found in Table 1. Steady-state solutions to the problem, pressure and superficial velocity contours, are shown in Figs. 3 and 4 respectively. The main pressure drop and the pinnacle of superficial velocity noticed for the system are located near the head distributors, as Figs. 3 and 4 show. Interestingly, Fig. 3 displays that screens/scallops/beds do not sharply increase in the pressure drop. Details reveal that the vortices at the upper region of reactors do not enter into the beds and all become damped down before passing through the porous media. Superficial velocity

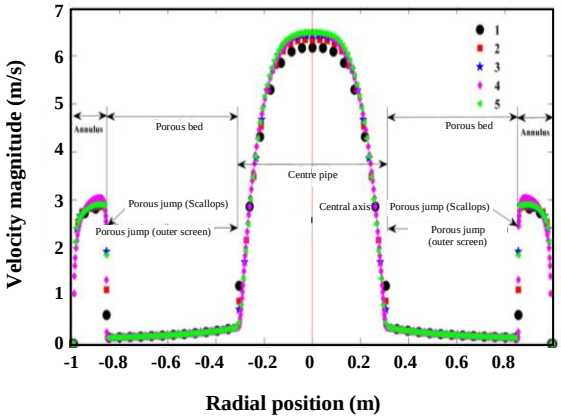

Fig. 2: Velocity profile obtained for five different grids in a given cross section of the first reactor.

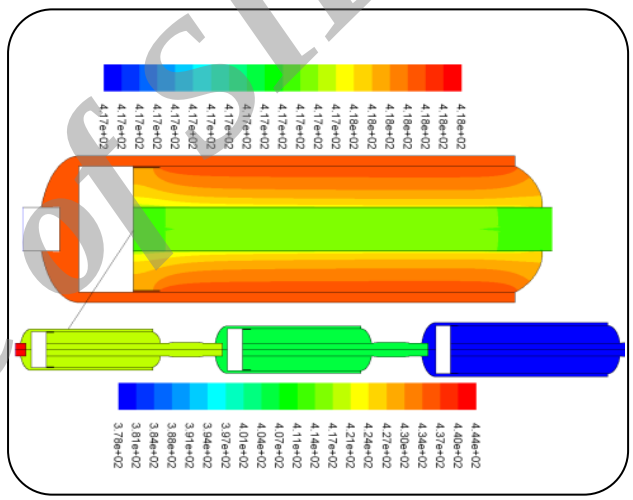

Fig. 3: Contours of relative pressure (Psig).

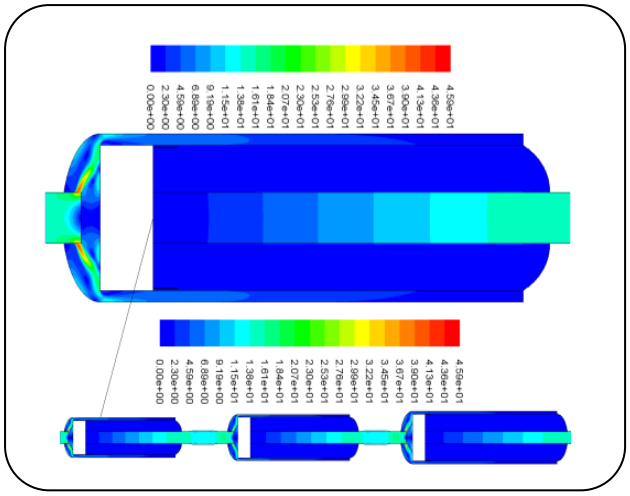

Fig. 4: Contours of velocity magnitude (m/s).

vectors in Fig. 5 verify this claim. Regarding improvement of hydrodynamics, there are two parameters to be set adjacent to their optimal points; one is to minimise pressure drop and the other is making flow distribution uniform through catalytic beds. Radial uniformity along the bed distributors results in not only pressure drop reduction but also higher conversion; hence, the most crucial problem remains for uniformity. The property of uniform fluid distribution can at any given time be checked more discernibly by tracing stream lines, which usually gives us a new sight of distribution as shown in Fig. 6. From this figure, it seems that there are recirculating fields at the end of each reactor, where the outer screen, centre pipe, and outlet connect. The fields have been strengthened from the first to the last reactor. The cause of this phenomenon is perhaps the insufficient pressure gradient between upstream and downstream of each bed. For quantitative showing, radial velocity at the boundaries of every bed is plotted against the position (Fig. 7). Positive radial velocity at the outer screens denotes the existence of a recirculation or back-mixing region. The best design of screens will give us a uniform/flat plot of radial velocity with continuous negative values along the position; i.e. the flatter the plot of radial velocity, the more uniform fluid distribution. Without any significant difference in essence, the major aim of CFD improvement may shift to this subject (uniformity). A summary of results in this section can be found in Table 3. As can be seen, the predicted results are in good agreement with those under design conditions so that the maximum relative error obtained is less than 3%. As is clear from Table 4, the deviation of results from Ergun equation for the first and second beds is less than 20%, which is acceptable through the framework of engineering, while for the third reactor, it increases to 54% because of the sharp back-mixing at the end of its bed. Round the shield at the top of each bed and the centre pipe at the end of each bed are suspected to be agents of great deviance.

Current conditions

Unlike the design conditions, detailed study on the system under current/working conditions reveals that the first reactor with crucial distribution problem has to be revamped as soon as possible. Fig. 8 shows that the first reactor has serious flow distribution problems along its bed,

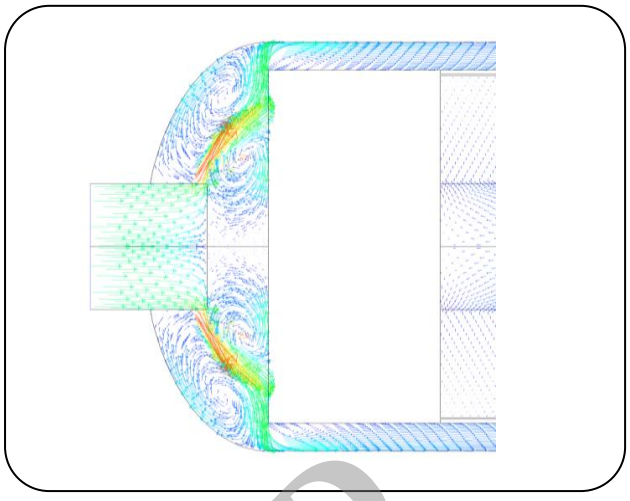

Fig. 5: Superficial velocity vectors at top section of the first reactor.

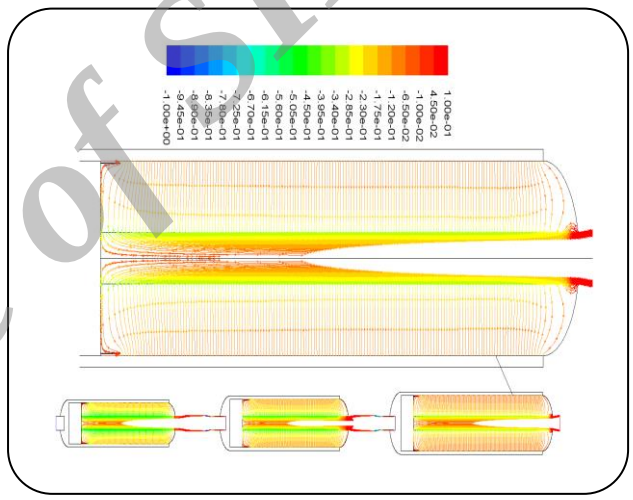

Fig. 6: Stream lines coloured by radial velocity (m/s).

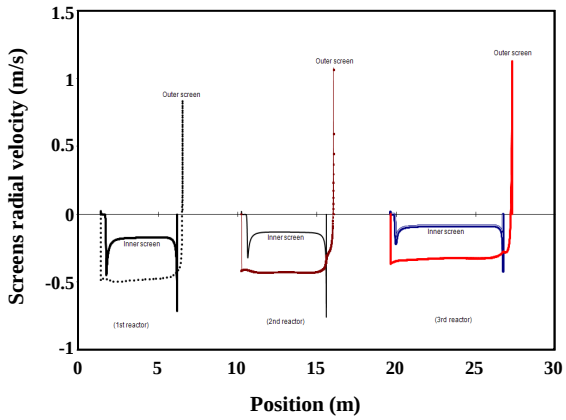

Fig. 7: Radial velocity profile along the bed distributors.

Table 3: Predicted pressure/pressure drop compared to the design data.

Statement	P_1^{in} (Psig)	P_1^{out} (Psig)	P_2^{in} (Psig)	P_2^{out} (Psig)	P_3^{in} (Psig)	P_3^{out} (Psig)	ΔP_{total} (Psig)
Predicted	443.76	417.33	417.31	404.28	404.26	378 (set)	65.76
Design	445	428	415	406	395	378	67
%RE[1]	0.28	2.5	0.57	0.42	2.34	0	1.85

1) The percentage of relative error is calculated from; $RE\% = \frac{|M_{Exp} - M_{Pred}|}{M_{Exp}} \cdot 100$, *where M refers to a fluid property.*

Table 4: Predicted pressure drop compared to that calculated by Ergun equation.

Bed No.	$(\Delta P/L)_{pre}$ (Psi/m)	$(\Delta P/L)_{Erg}$ (Psi/m)	%RE
1	0.5620	0.4876	15.26
2	0.4285	0.3584	19.56
3	0.3454	0.2230	54.89

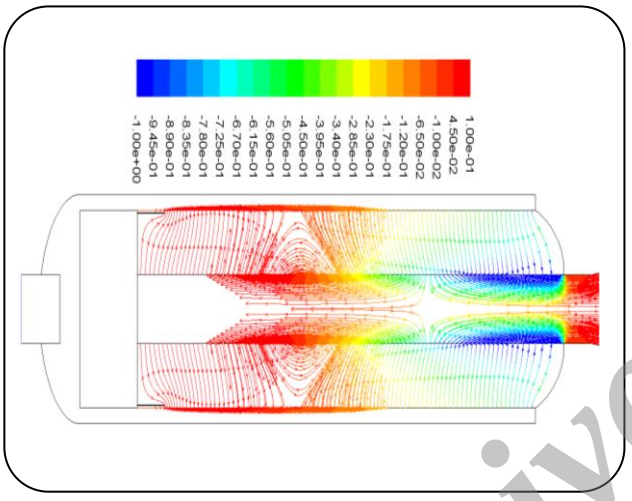

Fig. 8: Stream lines coloured by radial velocity (m/s) in the first reactor.

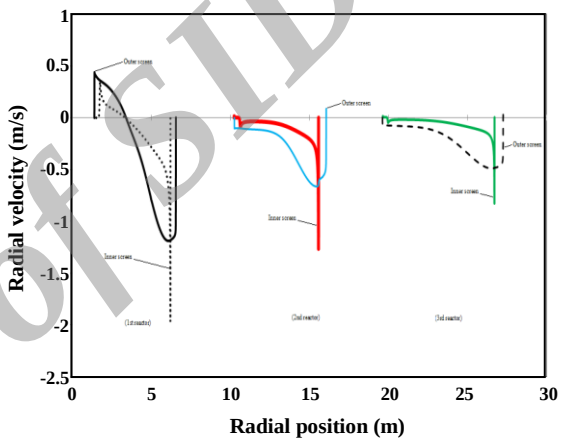

Fig. 9: Radial velocity profile along the bed inner/outer screens.

in a way that nearly half of its bed is useless. We shall see that a perspicacious solution to this problem may be capacity enhancement. Radial velocity profiles for reactors versus position along their inner/outer screens are depicted, as one can observe in Fig. 9, where an uneven profile for the first reactor is quite distinct from others. Once again, validation upon pressure drop is reported (Tables 5 and 6). From Tables 3-6, it can be understood that the error of calculation under working conditions is generally less than the one under design conditions due to superior flow distribution (except for the first reactor).

Porosity distribution

Evaluating local porosity within a packed column has actively been one of the great interests of scientists for many years. Empirical techniques to measure porosity distribution were listed [30]. Several discrete element methods for an assembly of randomly packed particles, were developed by considering various particle to bed diameters (d/D) [31-33]. We found that de *Klerk et al.* [34] have best fitted their relation upon experimental data for radial porosity distribution in pipes with different particle to pipe diameters:

$$\text{Local porosity} = \varepsilon(r) = \varepsilon_b + 0.29\exp(-0.6\frac{R-r}{d})\left[\cos\left(2.3\pi\left(\frac{R-r}{d}-0.16\right)\right)\right] + 0.15\exp\left(0.9\frac{R-r}{d}\right) \quad (10)$$

Table 5: Predicted pressure/pressure drop under current conditions compared to the experimental data.

Description	P_1^{in} (psig)	P_1^{out} (psig)	P_2^{in} (psig)	P_2^{out} (psig)	P_3^{in} (psig)	P_3^{out} (psig)	ΔP_{total} (psig)
Exp. data	420	418	402	398	395	390	30
Predicted	419.60	408	407.86	401	399.59	390 (set)	29.60
RE%	0.1	2.39	1.46	0.76	1.16	0	1.33

Table 6: Predicted pressure/pressure drop under current conditions compared to the Ergun equation.

Bed No.	$(\Delta P/L)_{pre}$ (psi/m)	$(\Delta P/L)_{Erg}$ (psi/m)	%RE
1	0.4423	0.3648	21.24
2	0.2885	0.2437	18.38
3	0.2249	0.1539	46.13

The correlation is plotted for *R/d*=40 (Fig. 10). The figure shows that 0.02 m away from the wall and farther, oscillations in the radial distribution weaken and the function approaches 0.37 as expected porosity. Thus channelling can be searched only very close to the wall boundary. Therefore, a fine grid near the wall is essential. The channelling causes large variations in velocity profile, heat transfer, short contact time and non-uniform head loss along the packed bed [35]. Eq. (10) provides only the one-sided profile through the packed domain. In this paper, a novel symmetrical porosity distribution is used for the annulus space. To the best of our knowledge, such symmetrical distribution has been introduced in this work for the first time. To probe effects of porosity distribution on the flow characteristics, several runs are established under both design and working modes. The parameter of volume-weighted average of physical velocity magnitude is defined as:

$$\bar{v} = \frac{1}{V}\int_v v_i dV = \frac{1}{V}\sum_{i=1}^{n} v_i V_i \qquad (11)$$

The index *i* progresses towards *n* (i.e. summation over all cells). Lower velocity leads to lower pressure drop across the bed, which is completely what Eq. (8) emphasises. Although this conclusion might be true in most cases, it is worth noting if the conclusion is made only on the basis of the velocity magnitude, e.g. the form of flow field and vortices have been ignored. For example, for the bed No.2, the velocity in the case of constant porosity is less than the one in the case of distributed porosity, while the relevent pressure drop for constant porosity case is higher. At first glance,

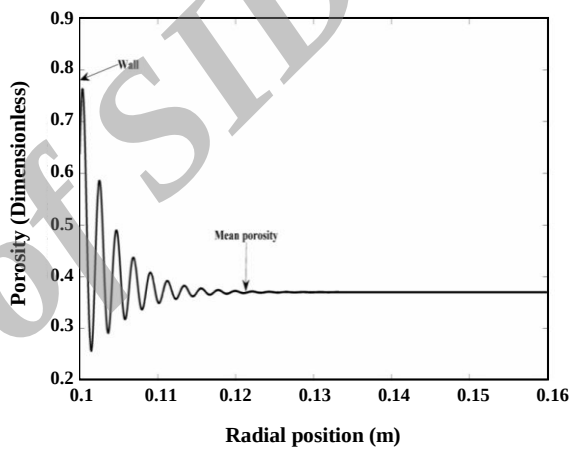

Fig. 10: Radial porosity distribution for R/d=40.

this is contradictive with the Ergun equation. But since the Ergun equation has supposed that no back-mixing and vortex exist through the domain, the opposition can be explained. It is found that the system charged with a symmetrical particle distribution operates more ideal (has lower pressure drop and superior flow distribution) than that of constant porosity. Channelling occurs, anyway, in case of porosity distribution, but it is negligible. An idea to show channelling might be to follow velocity angle at the boundaries of each bed (scallops/screens). If the angle is around 180°, channelling is playing the main role, and if it is approximately 90°, the channelling is negligible.

Distributor redesign

According to Fig. 3, the main pressure drop through the system is because of head distributors. Commonly,

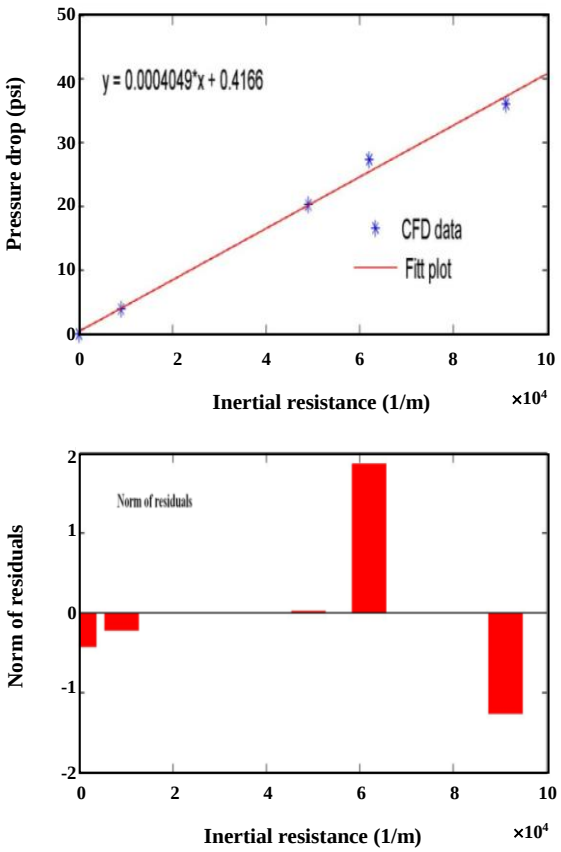

Fig. 11: Correlation of distributor pressure drop versus inertial resistance.

fluid distributor, like a perforated plate, contains several rows of tiny holes arrayed on typical pitch, e.g. delta or square pitch. The most important factor in the field of distributor design is setting the open area proportional to the input flow rate. Two rows of 19 mm holes arranged on 25 Δ pitch have been designed for all head distributors. To calculate hydrodynamic resistance of the distributor, we ignor the contribution of viscous resistance (diffusion resistance) due to high *Re* number in the holes. Inertial resistance can be calculated in the following form:

$$C = \frac{1}{C_0}\frac{\left(\frac{A_t}{A_o}\right)^2 - 1}{t} \qquad (12)$$

Where C_0 can be represented as a function of hole Re number. For high Re, the value of C_0 is near the unit [36]. Altering the open area, we are able to reach lower inertial resistance and pressure drop, thereby reducing the wastage of energy resources. Up to 5 runs are implemented to derive a useful relation between pressure drop and inertial resistanse. An adjusted R-squared above 0.99 is obtained from the fitting procedure (Fig. 11) on at least 5 data points. The correlation is:

$$\Delta P = 0.0004049C + 0.4166 \qquad (13)$$

In general, we can afford increments in the open area and this action decreases in the pressure drop across the distributor, as mentioned before.

Screen redesign

It is possible to attain superior flow distribution through the catalytic beds by means of screen redesign. Based on the various inertial resistances for scallops and outer screens, simulations are performed. It is found that scallops are working under ideal mode with low pressure drop and do not have influence over flow distribution. Instead, on the opposite side of the beds where outer screen exists, the flow field depends largely on the screen inertial resistance. As a result, when inertial resistance of respective outer screen increases, the intensity of vortices at the end of catalytic bed diminishes. The recirculating field at the end of catalytic beds, especially in the third reactor, will be removed if inertial resistances increase fourfold in value, albeit reluctantly due to increase in the pressure drop. In Table 7, effect of inertial resistance increase on the pressure drop is elucidated. Radial velocity profile shows some positive values, representative of back-mixing regions, which become damped down towards zero with resistance increase. It seems that an increase in the inertial resistance somewhat leads to larger pressure drop. How much pressure drop do we have with outer screen resistance increase? To comprehend how much it changes, the data of pressure drop against inertial resistance is displayed in Table 7, exhibiting that increases in inertial resistance do not result in heavy pressure drop.

Porosity effect

Densely packed particles decrease not only in the propability of channelling phenomenon, but also in the flow mal-distribution, even though they increase in the pressure drop. Large particle-free area in the bed, high void fraction, would be undesirable because it diminishes active surface of reactions. Turbulence generation and

Table 7: Predicted pressure/pressure drop for different inertial resistances.

Inertial resistance of outer screen	Inertial resistance of scallop	$(\Delta P/L)_1$ (psi/m)	$(\Delta P/L)_2$ (psi/m)	$(\Delta P/L)_3$ (psi/m)	ΔP_{total} (psi)
Normal	Normal	0.5620	0.4285	0.3454	65.76
Normal	2-fold	0.5653	0.4287	0.3452	65.85
2-fold	Normal	0.5662	0.4292	0.4243	66.02
3-fold	Normal	0.5668	0.4298	0.5008	66.31
4-fold	Normal	0.5671	0.4304	0.5777	66.64

Table 8: Inertial/viscous resistances and CFD pressure drop for various porosities.

Mean porosity	Viscous resistance ($1/m^2$)	Inertial resistance (1/m)	ΔP_{total} (psi)
0	∞	∞	∞
0.1	4.8211e10	1.9843e6	143.95
0.2	4.7616e9	2.2047e5	72.81
0.3	1.0802e9	5.7160e4	66.72
0.37	4.6638e8	2.7421e4	61.59
0.5	1.1904e8	8.8189e3	62.75
0.6	4.4089e7	4.0828e3	62.64
0.7	1.5618e7	1.9283e3	62.60
0.8	4.6500e6	8.6122e2	62.59
0.9	8.1646e5	3.0243e2	61.89
1	0	0	0

dissipation rates in such sytems (high porosity) are not equivalent. Ultimately, the beds with high porosity have the problem of fluidity due to the movement of embeded fine particles.

Nine values between 0 and 1 are intended to carefully investigate how pressure drop will change with porosity. Corresponding inertial/viscous resistances and CFD pressure drop data are computed and incorporated in Table 8, where the table bears a physical meaning; as $\varphi \rightarrow 0$ then $\Delta P_{total} \rightarrow \infty$. More importantly, there is no salient difference in the pressure drop when the prosity range is between 0.2-0.5. This range is practically available. Hence, we can choose a value in the range to improve flow distribution without worrying about the levels of total pressure drop. The proportion of volume weighted average of radial velocity to that of velocity magnitude in each bed is a relatively good criterion for flow uniformity:

$$\%U = \frac{|\bar{v}_R|}{|\bar{v}|}.100 \qquad (14)$$

Uniformity parameter decreases with porosity increase as Table 9 shows. Low porosity can entirely remove mal-distribution and obviously can increase in the rate of reactions by the increases in active surface area. Radial velocity profile and stream lines reveal that mal-distribution is removed for porosity of 0.2 and flow distribution becomes almost uniform. Besides, the intensity of recirculating flow at the end of catalytic beds for φ=0.2 is much lower than that of φ=0.37.

Capacity enhancement

Several runs under different inlet mass flow rates are carried out looking for a likely optimal capacity under which flow distribution is uniform. Advantageously, other limitations such as reaching maximum endurable pressure (threshold value), which is very crucial from point of view of HSE, would be discovered whilst growing in the flow rate. The examined inlet velocities are 11.533, 15.848, 25, 31.696, 47.544 and 55 m/s. Of the

Table 9: Volume weighted average of velocity magnitude, radial velocity, and uniformity parameter.

Mean porosity	$\bar{v}_1$ (m/s)	$\bar{v}_{1,R}$ (m/s)	% U_1	$\bar{v}_2$ (m/s)	$\bar{v}_{2,R}$ (m/s)	% U_2	$\bar{v}_3$ (m/s)	$\bar{v}_{3,R}$ (m/s)	% U_3
0.1	0.2569	0.2532	98.55	0.2026	0.1994	98.41	0.1367	0.1354	98.98
0.2	0.2571	0.2533	98.52	0.2027	0.1994	98.39	0.1367	0.1354	98.98
0.3	0.2573	0.2533	98.44	0.2028	0.1994	98.33	0.1368	0.1354	98.93
0.37	0.2578	0.2535	98.35	0.2025	0.1989	98.25	0.1371	0.1354	98.78
0.5	0.2580	0.2533	98.16	0.2033	0.9994	98.05	0.1371	0.1354	98.73
0.6	0.2585	0.2533	97.98	0.2038	0.1995	97.87	0.1373	0.1354	98.60
0.7	0.2598	0.2533	97.50	0.2046	0.1994	97.44	0.1378	0.1353	98.20
0.8	0.2630	0.2533	96.30	0.2070	0.1994	96.33	0.1395	0.1354	97.05
0.9	0.3039	0.2544	83.71	0.2245	0.1990	88.63	0.1568	0.1355	86.41
1	1.3529	0.2531	18.71	1.0740	0.1982	18.46	0.8394	0.1353	16.12

mentioned velocities, two first values corrspond to working and design conditions respectively. They should be compared together apart from visionary inlet velocities. In the course of simulation, it is found that operating pressure of each reactor, as well as pressure drop quantity, largely depend on the inlet mass flow rate. The simplest way to eliminate mal-distribution and back-mixing fields may be manipulation of inlet velocities, which are economically useful (more profitability), because it does not work either with internal (screen/scallop/distributor) redesign or with porosity changes. Several runs associated with higher inlet velocities are performed. In the meantime, operating pressure as an important HSE factor and radial velocity profile are frequently checked to prevent system from explosion and to hypothetically reach the optimal flow distribution. Fortunately, we find that there is an optimal inlet velocity under which appropriate flow distribution together with capacity enhancement are conceivable. Indeed, we notice that radial velocity profile becomes rougher with velocity increase until $v_{in}=53$ *m/s* is attained. After that, the profile tends towards smoothness. As is seen in Fig. 12, the profile loses its smoothness when velocity increases until $v_{in}=53$ *m/s* and starts being smoothed over the screen position, afterwards. Pressure drop and volume weighted average of velocity magnitude are reported in Table 10, where the relative deviation of CFD pressure drop from that calculated by Ergun equation is included. Arbitrary capacity enhancement is not allowed unless the gained pressure through

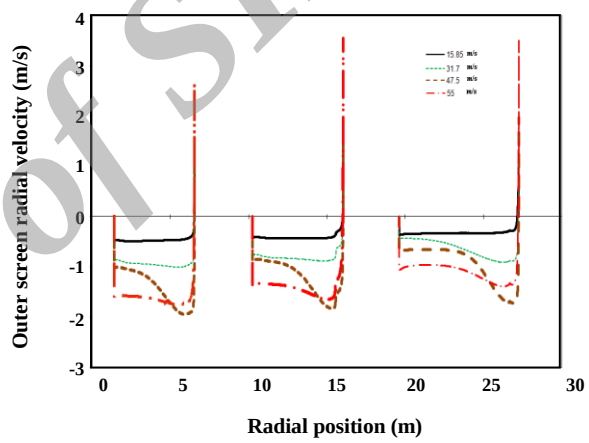

Fig. 12: Radial velocity profile along the outer screens for different inlet velocities.

the system does not exceed the maximum hydrostatic pressure. The percentage of confidence margin of operation is defined as:

$$\%Con = \frac{P_{max-allowed} - P_{calc}}{P_{max-allowed}}.100 \qquad (15)$$

As Eq.15 explains, a large confidence margin signifies safer operatinal conditions. Quantitative details about confidence bound of hydrostatic pressure can be found in the table beneath (Table 11), where it is clear that we can have at most an inlet velocity of 55 m/s. Larger inlet velocity can be damaging and explode the system.

Table 10: Pressure drop obtained from CFD simulation under different inlet velocities in comparison to that predicted by Ergun equation.

v_{in} (m/s)	$(\Delta P/L)_1$ (psi/m)	$(\Delta P/L)_{1,Ergun}$ (psi/m)	$(\Delta P/L)_2$ (psi/m)	$(\Delta P/L)_{2,Ergun}$ (psi/m)	$(\Delta P/L)_3$ (psi/m)	$(\Delta P/L)_{3,Ergun}$ (psi/m)	$\%RE_1$	$\%RE_2$	$\%RE_3$
15.848	0.5620	0.4876	0.4285	0.3584	0.3454	0.2230	15.26	19.56	35.43
31.696	1.5064	1.2637	1.1115	0.9009	1.0190	0.5301	19.21	23.38	92.23
47.544	2.9764	2.3505	2.1901	1.6355	2.1168	0.9301	26.63	33.91	127.59
55	3.5846	2.9462	2.5828	2.0305	2.4217	1.1298	21.67	27.20	114.35

Table 11: CFD pressure drop, operating pressure and confidence bound under different inlet velocities.

v_{in} (m/s)	$(\Delta P/L)_{total}$ (psig)	P^1 (psig)	P^2 (psig)	P^3 (psig)	$\%Con^1$	$\%Con^2$	$\%Con^3$
15.848	65.76	443.76	417.34	404.29	60.20	65.04	61.71
31.696	261.40	639.40	527.71	483.11	42.65	55.77	54.25
47.544	588.35	966.35	730.18	617.17	13.33	38.79	41.56
55	789.41	1167.41	850.78	693.74	0	28.69	34.30

Turbulency in bed

In order to investigate the effect of turbulence on the hydrodynamics and flow distribution, several cases are run in which the major turbulence parameters, namely turbulence generation rate and turbulence dissipation rate (specifically for k-ε model) are permitted to be calculated through the porous media. Results show that recirculating fields at the end of catalytic beds vanish under turbulent regime. Therefore, conversion has to be higher than the previous strategy (laminar flow pattern in the bed), as recognised [37]. Although turbulent flow eliminates back-mixing fields, flow distribution along the beds seems to be less uniform, as Fig. 13 shows. Oddly enough, a new undesirable recirculating field near the shields is found. The data of pressure drop in the beds obtained by CFD simulations for both laminar and turbulent regimes and pressure drop calculated by Ergun equation are listed in Table 12. It is obvious that pressure drop in case of turbulent regime is higher than that of laminar regime. Details show that the assumption of turbulent flow in the beds somehow results in larger velocity magnitude there. It also decreases the uniformity parameter.

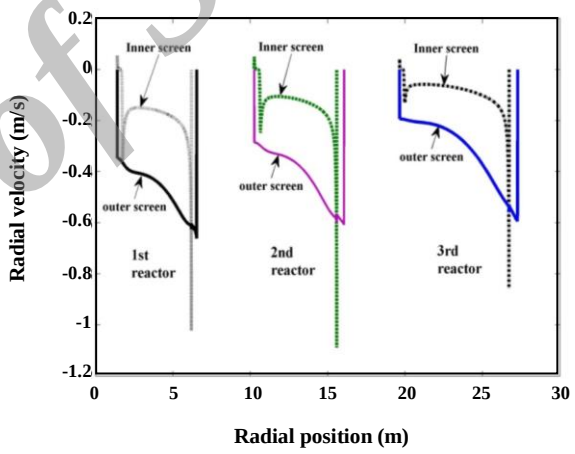

Fig. 13: Radial velocity profile along the inner/outer screens obtained under the assumption of turbulent flow through catalytic beds.

Geometry modification

The excellent relationship between CFD simulation and fluid dynamics, which is dependent on the geometry, makes this group of simulations more and more effective. That is why CFD simulation has widely attracted interest. Normally, each reactor has a shield at the top of its bed. Its function is sealing the bed against the axial flow and preventing flow from short circulating. By removing the shield, we can probably obtain superior radial flow distribution through porous bed. We can have our say in decision-making process via geometry midification. In the first step, one may take the shield out of reactor. The second step may be to fill free space (catalyst free zone) obtained by shield elimination with fresh catalyst, i.e. the extension of catalytic bed. Fictitious modified geometries, accompanied

Table 12: CFD pressure drop for different flow regime through the beds in comparison to that predicted by Ergun equation.

Flow regime	$(\Delta P/L)_1$ (psi/m)	$(\Delta P/L)_2$ (psi/m)	$(\Delta P/L)_3$ (psi/m)
Laminar	0.5620	0.4285	0.3454
Turbulent	0.5858	0.4542	0.3807

Table 13. Pressure drop across the fist bed for different geometries.

Geometry	a	b	c
Pressure drop per length (Psi/m)	0.5466	0.5620	0.4623

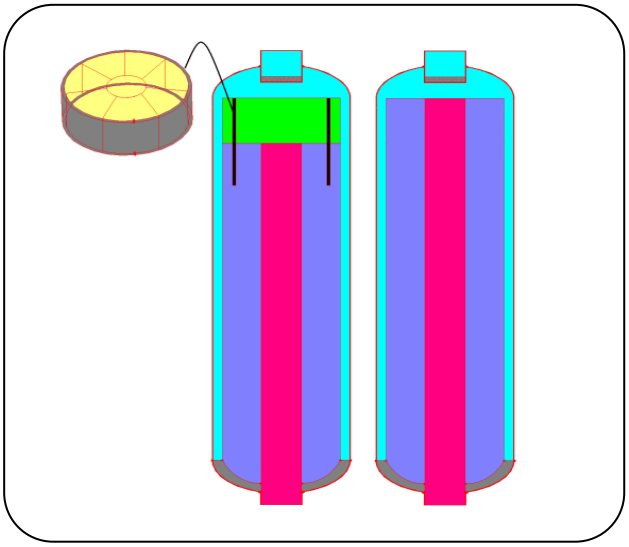

Fig. 14: The genuine (left hand) and shield removed with extra loading (right hand) reactors.

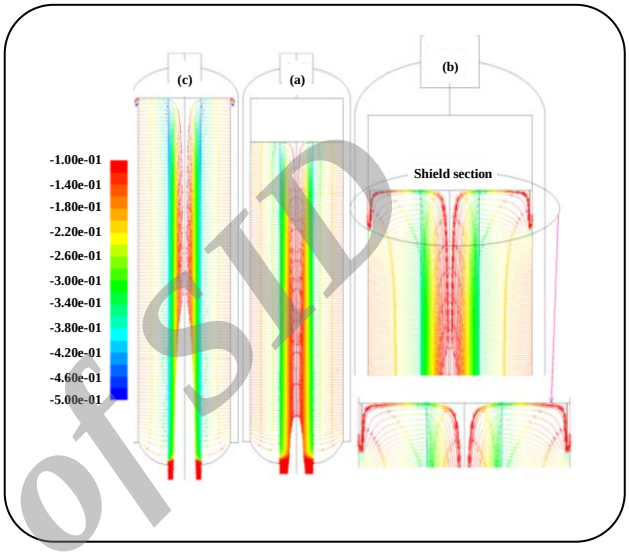

Fig. 15: Stream lines for (a) removed shield, (b) genuine and (c) extra loaded reactors.

by the genuine system, are exhibited in Fig. 14. Although case (a) gives us a desired radial distribution, it has an unloaded area with a lot of disadvantages (see Fig. 15). The best case remained is case (c) that bears extra catalyst loading and contacts between fluid-catalyst over longer period of time, which is straightforwardly proportioned to the conversion. CFD simulations reveal that for case (c) radial velocity contours are better distributed than others. Nevertheless, some defected zones located at the end of catalytic beds are observed. Stream lines in Fig. 15 confirm the above consequence showing that the path lines adjucent to the shield (case b) deviate from normal radial pattern. They are as radial for case (c) as for case (a). Applying this technique, we succeed in loading 15-20 volume per cent in addition to current catalyst loading, as others did [38]. More interestingly, a lower pressure drop across porous bed is the inevitable result of removing the shield (See Table 13).

CONCLUSIONS

Several runs with different conditions are examined in order to predict reactor pressure drop. Results show good agreement with the experimental data. Simulations show that the major part of pressure drop is induces by head distributors. Results show a good radial flow distribution for the system under design conditions and an undesirable one for the system under current (working) conditions. However, defected zones at the end of each bed for both conditions are observed, but they vanish with increases in the inertial resistance of outer screens, increase in the inlet velocity and decrease in the bed prosity. The first reactor under the working conditions needs substantial revising by capacity enhancement, which heals flow distribution through the first bed and removes recirculating flow field. Optimal bed porosity is found to be about 0.2. At last, it is found that between 15-20% enhancement in catalyst loading and volumetric flow rate are accessible by modifying geometry.

Nomenclature

A_o	Open area, m^2
A_t	Total area, m^2
C	Inertial loss, 1/m
C_0	Discharge coefficient, dimensionless
Con	Confidence bound, dimensionless
D	Viscous loss, $1/m^2$
D_p , d	Particle diameter, m
F	Momentum source term, N/m^3
L	Characteristic length, m
P_{calc}	Calculated pressure, N/m^2
$P_{max\text{-}allowed}$	Maximum hydrostatic pressure, N/m^2
R	Pipe radius, m
r	Radial coordinate, m
S_m	Mass source term, $kg/(m^3.s)$
t	Thickness, m
U	Uniformity parameter, dimensionless
V	Volume, m^3
x	Axial coordinate, m
ρ	Density, kg/m^3
ν	Velocity, m/s
ν_z	Swirl velocity component, m/s
$\|\nu\|$	Velocity magnitude, m/s
μ	Viscosity, kg/(m.s)
α	Permeability, m^2
φ	Porosity, dimensionless
ϕ_p	Sphericity, dimensionless
ε	Local porosity, dimensionless
ε_b	Bulk porosity, dimensionless
ΔP	Pressure drop, N/m^2

Received : Mar. 5, 2012 ; Accepted : Apr. 28, 2014

REFERENCES

[1] Ranade V.V., "Computational Flow Modeling for Chemical Reactor Engineering", Academic Press, London (2002).

[2] Zafar Q., Gevert B., von Sivers M., Statistical Model for Benzene Prediction in Catalytic Reforming, *Prepr. Pap. -Am. Chem. Soc., Div. Fuel Chem.*, **48**: 2-660 (2003).

[3] Boyas R.S., Froment G.F., Fundamental Kinetic Modeling of Catalytic Reforming, *Ind. Eng. Chem. Res.*, **48**: 1107-1119 (2009).

[4] Fazeli A., Fatemi Sh., Mahdavian M., Ghaee A., Mathematical Modeling of an Industrial Naphtha Reformer with Three Adiabatic Reactors in Series, *Iran. J. Chem. Chem. Eng. (IJCCE)*, **28**: 97 (2009).

[5] Fortuny A., Bengoa C., Font J., Castells F., Fabregat A., Water Pollution Abatement by Catalytic Wet Air Oxidation in a Trickle Bed Reactor, *Catalysis Today.*, **53**: 107-114 (1999).

[6] Froment G.B., Bischoff K.B., "Chemical Reactor Analysis and Design", Wiley & Sons, New York (1990).

[7] Raskin A.Y., Sokolinskii Y.A, Mukosei V.I., Aerov M.E., *Theor. Found. Chem. Techn [in Russian].*, **2**: 220 (1968).

[8] Panahandeh M.R., Fathikaljahi J., Taheri M., Steady-State Modeling and Simulation of an Axial-Radial Ammonia Synthesis Reactor, *Chem. Eng. Technol.*, **26**: 666-671 (2003).

[9] Liang K.M., Guo H.Y., Pan S.W., A study on Naphtha Catalytic Reforming Reactor Simulation and Analysis, *J. Zhejiang. Univ. Sci.*, **6B**: 590-596 (2005).

[10] Hlavacek V., Kubicek M., Modeling of Chemical Reactors-XXV: Cylindrical and Spherical Reactor with Radial Flow, *Chem. Eng. Sci.*, **27**: 177-186 (1972).

[11] Calo J.M., Cell Model Studies of Radial Flow, Fixed Bed Reactors, *ACS. Symp. Ser.*, **65**, 550 (1978).

[12] Genkin V.S., Dil'man V.V., Sergeev S.P., The Distribution of a Gas Streem Over a Radial Contact Apparatuos, *Int. Chem. Eng.*, **13**: 24- (1973).

[13] Ponzi P.R., Kaye L.A., Effects of Flow Maldistribution on Conversion and Selectivity in Radial Flow Fixed-Bed Reactors, *AIChE. J.*, **25**: 100-108 (1979).

[14] Chang H.C., Calo J.M., An Analysis of Radial Flow Packed Bed Reactor, *ACS Symp. Ser.*, **168**, 305 (1981).

[15] Lobanov E.L., Skipin Y.L., Increasing the Operating Efficiency of Radial Reactors in Reforming, *Chem. Tech. Fuels Oil.*, **22**: 275- (1986).

[16] Nooy F.M., Dense Loading, *Oil & Gas Journal.*, **82**: 152- (1984).

[17] Song X., Wang Z., Jin Y., Gong M., Investigations on Hydrodynamics of Radial Flow Moving Bed Reactors, *Chem. Eng. Technol.*, **16**: 383- (1993).

[18] Heggs P.J., Ellis D.I., The Modeling of Fluid-Flow Distribution in Aannular Packed Beds, *Gas Sep. & Pur.*, **8**, 257 (1994).

[19] Bolton G.T., Hooper C.W., Mann R., Stitt E.H., Flow Distribution Measurement in a Radial Flow Fixed Bed Reactor Using Electrical Resistance Tomography, "Proceedings of 17th International Symp. On Chem. Eng.", Hong Kong, (2002).

[20] Ranade V.V., Improve Reactor via CFD, *Chem. Eng. (An Indian J).*, **104**: 96- (1997).

[21] Mohammadikhah R., Ziyari A., Behjat Y., Ahmadi-Marvast M., Ayazi M., Nikbakht M., Removing Mal-Distribution Through a Radial-Flow Fixed Bed Reactor using CFD, "Proceedings of 6th Int. Chem. Eng. Cong.", Iran (2009).

[22] Mohammadikhah R., Behjat Y., Ahmadi-Marvast M., Nikbakht M., Ganji H., CFD Application in Capacity Enhancement of Naphtha Catalytic Reforming Unit of Tehran Refinery, "Proceedings of 14th Int. Oil. Gas. Petrochem. Cong.", Iran (2010).

[23] Mohammadikhah R., Ganji H., Ahmadi-Marvast M., Zahedi Abghari S., Turbulence Model Inspection for Hydrodynamics of Naphtha Catalytic Reactors, "Proceedings of 7th Int. Chem. Eng. Cong.", Iran (2011).

[24] Mohammadikhah R., Zahedi Abghari S., Ahmadi-Marvast M., Ganji H., Simulation of Hydrodynamic and Heat Transfer Phenomena in Catalytic Reforming Reactors via CFD, *Petroleum Science & Technology journal [In Persion]*, **73**: 25-44 (2012).

[25] Mohammadikhah R., Zahedi Abghari S., Ahmadi-Marvast M., Ganji H., CFD Simulation of Catalytic Naphtha Reforming Process, "7th International Chemical Engineering Congress & Exihibition", 21-24 November, Kish Island, Iran, (2011).

[26] Carman P.C., Fluid Flow Through Granular Beds, *Trans. Inst. Chem. Eng.*, **15**: 150- (1937).

[27] Ergun S., Flow Through Packed Columns, *Chem. Eng. Prog.*, **48**: 89- (1952).

[28] Mehta D., Hawley M.C., Wall Effect in Packed Column, *Ind. Eng. Chem. Proc. Des. Dev.*, **8**: 280- (1969).

[29] Geertsma J., Estimation the Coefficient of Inertial Resistance in Fluid Flow Through Porous Media, *SPE. J.*, **14**: 445- (1974).

[30] Hosseini-Ashrafi M.E., Tuzun U., A Tomographic Study of Voidage Profiles in Axially Symmetric Granular flows, *Chem. Eng. Sci.*, **48**: 53- (1993).

[31] Zhang Z.P., Liu L.F., Yaun Y.D., Yu A.B., A Simulation Study of the Effects of Dynamic Variables on the Packing of Spheres, *Powder Technology.*, **116**: 23- (2001).

[32] P. Cundall and O.D.L. Strack, A Discrete Element Model for Granular Assemblies, *Geotechnique.*, **29**: 47- (1979).

[33] Theuerkauf J., Witt P., Schwesig D., Analysis of Particle Porosity Distribution in Fixed Beds Using the Discrete Element Method, *Powder Technology.*, **165**: 92- (2006).

[34] De Klerk A., Voidage Variation in Packed Beds at Small Column to Particle Diameter Ratio, *AIChE J.*, **49**: 2022- (2003).

[35] Freund H., Zeiser T., Huber F., Klemm E., Brenner G., Durst F., Emig G., Numerical Simulations of Single Phase Reacting Flows in Randomly Packed Fixed-Bed Reactors and Experimental Validation, *Chem. Eng. Sci.*, **58**: 903- (2003).

[36] Perry R.H., D.W. Green Eds., "Perry's chemical engineering handbook", 7th Ed, Mc Graw Hill, New York (1997).

[37] Levenspiel O., "Chemical Reaction Engineering", 2nd Ed, Wiley & Sons, New York (1972).

[38] Poussin B., Reactor with a Llower Wall and/or an Upper Wall Having a Layer of a Flexible Refractory Material, *US patent 5202097*, Apr. 13, (1993).